Use of Radio Frequency Identifiers in Autonomous Mobility Systems: with a Focus on Safety

João Mota Neto, Marcos Antônio Jeremias Coelho, Gabriela Rocha Roque, and Roderval Marcelino

***Abstract*—Autonomous mobility systems rely heavily on perception technologies to interpret road infrastructure and make driving decisions without human intervention. Among these technologies, camera-based traffic sign recognition systems are widely employed; however, their performance is significantly degraded under adverse conditions such as sign deterioration, partial occlusion, poor lighting, and vandalism. In countries with limited infrastructure maintenance, these conditions represent a critical safety risk. This work proposes and experimentally evaluates the use of Radio Frequency Identification (RFID) technology as a redundant perception layer for traffic sign identification in autonomous mobility systems. Passive UHF RFID tags were integrated into traffic signs and detected using a vehicle-mounted reader system. The experimental evaluation was conducted in two stages: controlled bench tests and field tests in a real campus environment. Bench tests resulted in a mean recognition distance of 10.35 m with a 95 % confidence interval of ±0.40 m, while field tests yielded a mean distance of 8.17 m with a confidence interval of ±1.05 m, influenced primarily by lateral sign offset and road geometry. All tagged signs positioned within the antenna's effective coverage area were detected during dynamic tests conducted at speeds of up to 40 km/h. A quantitative safety margin analysis demonstrates that the system cannot be used as a direct emergency braking trigger at speeds above 20 km/h, but is suitable as an anticipatory redundant perception layer at all tested speeds. A formal Bayesian sensor fusion framework is derived from the experimental data, and a dwell time analysis characterizes the EPCglobal Class 1 Generation 2 Slotted ALOHA protocol performance under dynamic conditions. A simplified Failure Mode and Effects Analysis (FMEA) is presented to support the safety argument. The results indicate that RFID-based perception is particularly suitable for controlled or semi-controlled environments where map-assisted pre-alerting is feasible.**

Link to graphical and video abstracts, and to code:
https://latamt.ieeer9.org/index.php/transactions/article/view/10693

***Index Terms*—Autonomous mobility, RFID, traffic sign identification, redundant perception, intelligent transportation systems.**

I. Introduction

THE development of autonomous vehicles has advanced significantly in recent years, driven by improvements in sensing technologies, embedded computing, and artificial intelligence. Current autonomous driving systems rely predominantly on vision-based perception to interpret road scenes, detect obstacles, and recognize traffic signs and signals [1], [2]. Despite notable progress, perception reliability remains one of the primary limiting factors for higher levels of driving automation, as defined by the SAE J3016 standard [3].

Traffic sign recognition systems based on computer vision and deep learning have demonstrated high accuracy under ideal conditions. However, their robustness is compromised by real-world factors such as adverse weather, poor illumination, occlusion by vegetation, vandalism, and physical degradation of signage [4], [5]. Experimental studies have shown that even minor visual alterations to traffic signs can lead to misclassification or complete recognition failure. These limitations are particularly relevant in developing countries, where infrastructure maintenance is often irregular [6].

In Brazil, a large proportion of roadways exhibit deficiencies in signage visibility and conservation. National surveys have reported a high incidence of missing, damaged, or obstructed traffic signs in Brazilian roadways. Under such conditions, vision-based autonomous perception systems may fail to interpret regulatory information correctly, leading to unsafe vehicle behavior [7].

Radio Frequency Identification (RFID) technology offers an alternative and complementary mechanism for object identification that is inherently independent of visual conditions. RFID systems have been widely adopted in logistics, access control, and vehicular identification applications due to their robustness, low maintenance requirements, and ability to operate under harsh environmental conditions [8]. Passive UHF RFID tags, in particular, do not require an onboard power source and can be deployed in outdoor environments with minimal maintenance [6], [9]. Recent advances in Infrastructure-to-Vehicle (I2V) communication have further demonstrated the viability of radio-frequency approaches for roadside information delivery in intelligent transportation systems [10]–[13].

This work investigates the application of RFID technology as a redundant traffic sign identification layer for autonomous mobility systems. By embedding RFID tags into traffic signs and equipping vehicles with suitable readers, it becomes possible to identify regulatory information regardless of visual degradation. The objective of this study is to experimentally evaluate the feasibility, performance limits, and practical constraints of such an approach under controlled and real-world conditions, contributing quantitative evidence to support its use as a safety-enhancing perception mechanism.

Unlike prior works that primarily address feasibility, the

The associate editor coordinating the review of this manuscript and approving it for publication was Cesar Azurdia (*Corresponding author: Marcos Antonio Jeremias Coelho*).

This study was financed in part by the Fundação de Amparo à Pesquisa e Inovação do Estado de Santa Catarina (FAPESC) – FAPESC 21/2024.

J. M. Neto, Marcos Antonio Jeremias Coelho, G. R. Roque are with Departamento de Engenharia Mecatrônica, Centro Universitário UniSATC, Criciúma, Brasil (e-mails: joao.neto@satc.edu.br, marcos.coelho@satc.edu.br, and gabriela.roque@satc.edu.br).

R. Marcelino is with Departamento de Computação, Federal University of Santa Catarina, Araranguá, Brasil (e-mail: roderval.marcelino@ufsc.br).

main contributions of this study are: (i) quantitative experimental characterization of RFID-based traffic sign recognition under dynamic and geometric constraints; (ii) a safety margin analysis combining recognition distance, latency, and vehicle dynamics; (iii) a Bayesian sensor fusion framework parametrized from experimental data; (iv) a dwell time and Slotted ALOHA protocol analysis under vehicular speeds; and (v) a simplified FMEA identifying the system's critical failure modes. Together, these contributions explicitly define the operational envelope of RFID-based redundant perception for autonomous mobility systems.

II. Experimental Procedure

This section describes the experimental methodology adopted to evaluate the feasibility and operational limits of an RFID-based traffic sign identification system used as a redundant perception layer for autonomous mobility applications. The experimental design was structured to ensure reproducibility and to allow direct comparison between controlled laboratory conditions and semi-controlled real-world environments.

The primary independent variables considered in this study are the distance between the vehicle-mounted antenna and the RFID tag, the lateral offset of the traffic sign relative to the vehicle trajectory, and the vehicle speed during dynamic tests [14]. Controlled variables include tag type, antenna model, mounting height, operating frequency, and communication protocol. The measured outputs are tag recognition occurrence, recognition distance, and detection consistency. Each test configuration was repeated multiple times to support statistical analysis.

A. RFID Reading Equipment

The RFID reading system employed in this study consists of a UHF integrated reader antenna (MID 12-iETH, Viaonda), operating in the 902–928 MHz frequency band, which is compliant with Brazilian regulations for UHF RFID systems. This frequency range is widely adopted in vehicular and logistics applications due to its favorable trade-off between reading range and robustness to environmental interference.

The antenna provides a nominal gain of 12 dBi and an approximate beamwidth of 42°. These characteristics are suitable for forward-looking vehicular perception, allowing selective detection of roadside infrastructure while limiting unintended tag detection outside the vehicle's lane of travel. Ethernet-based TCP/IP communication is used for data transmission, enabling reliable integration with onboard processing units. The selection of this antenna was based on compatibility with passive UHF tags, mechanical feasibility for vehicular installation, and stable communication performance under mobile conditions.

B. RFID Tag Configuration and Identification

Passive UHF RFID tags encapsulated in ABS material and rated IP68 were selected to ensure durability under outdoor exposure. The tags are designed for installation on metallic surfaces, which is compatible with typical traffic sign support structures. The operating temperature range of -30 °C to 80 °C further supports deployment in outdoor environments, covering the full operational range of Brazilian climate conditions.

Each tag stores a unique Electronic Product Code (EPC). Prior to installation, all tags were individually identified and cataloged using the manufacturer's configuration interface. The EPC codes were mapped to specific traffic sign categories within the processing software, in Fig. 1. Multiple tags were assigned to each sign type to improve detection reliability and to allow evaluation of simultaneous tag detection behavior. All 24 RFID tags were individually identified and cataloged, and the tag codes were assigned to each sign model in the developed program.

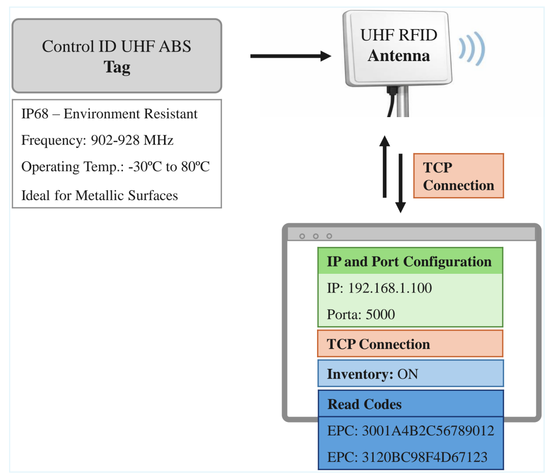

Fig. 1. System architecture overview: the Control ID UHF ABS passive RFID tag (IP68, 902–928 MHz, -30 °C to 80 °C) transmits its Electronic Product Code (EPC) wirelessly to the Viaonda MID 12-iETH UHF antenna, which forwards tag data via TCP/IP connection (IP 192.168.1.100, port 5000) to the processing unit. The Viaonda free reading interface displays the real-time EPC inventory used for tag cataloging prior to field deployment.

C. Information Processing Hardware and Software

The information processing subsystem was implemented on a Raspberry Pi single-board computer running a Linux-based operating system. The processing software was developed in Python and structured using a modular architecture to ensure deterministic behavior and ease of integration with other perception modules.

RFID data are received via TCP/IP communication, decoded, and mapped to predefined traffic sign categories. To avoid repeated detections of the same tag and to reduce communication overload, a fixed reading interval of 500 ms was implemented. This interval constitutes a deterministic upper bound on detection latency: no tag event can be processed before the next polling cycle. Multithreading was employed to decouple RFID data acquisition from higher-level processing tasks, ensuring continuous operation without blocking.

The system outputs symbolic representations of detected traffic signs, rather than raw RFID data, facilitating future sensor fusion and decision-making integration. Although timing stability was considered during system design, explicit end-to-end latency measurements were not conducted in the present study and are designated as future work; the safety implications of the polling interval are characterized analytically in Section IV.

Through the graphical interface, the system displays the image associated with the tag, followed by the priority level, the description of the sign model, and its corresponding code, as shown in Fig.2.

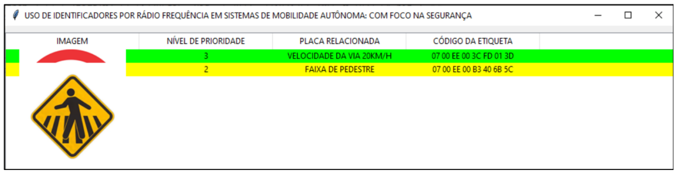

Fig. 2. Graphical user interface developed in Python for real-time RFID-based traffic sign identification. For each detected tag, the interface displays the corresponding sign image, the assigned priority level (1 = highest), the associated sign type, and the EPC code stored in the tag. The example shows the simultaneous detection of a speed limit and a pedestrian crossing sign.

Although timing stability was considered during system design, no explicit end-to-end latency measurements were performed. Therefore, the present evaluation focuses on recognition occurrence and distance rather than reaction-time suitability for safety-critical control.

D. Communication and System Integration Parameters

The RFID recognition module provides discrete digital outputs corresponding to detected traffic signs through the RPi.GPIO library, which allows access to the GPIO (General Purpose Input/Output) pins on the Raspberry Pi. Three digital outputs were configured, each corresponding to a specific traffic sign: STOP SIGN (GPIO Pin 18), PEDESTRIAN CROSSING (GPIO Pin 23), and 20 km/h SPEED LIMIT (GPIO Pin 24).

This communication strategy allows the RFID subsystem to function as an independent perception layer. Although sensor fusion was not implemented in this study, the adopted architecture supports future integration with vision-based or map-based perception modules without structural modification. The priority assignment implemented in this study reflects basic traffic safety hierarchy and was introduced exclusively to manage simultaneous detections at the perception layer.

E. Test Environments and Experimental Protocols

Two experimental environments were defined. The first consists of controlled bench tests, as shown in Fig.3, conducted in a laboratory setting, where tag orientation, alignment, and distance could be systematically adjusted. The second consists of field tests conducted on a predefined route within a university campus, representing semi-controlled real-world conditions.

For the application of the RFID-based traffic sign recognition test in a controlled environment, three traffic sign models: a STOP sign, a PEDESTRIAN CROSSING sign, and

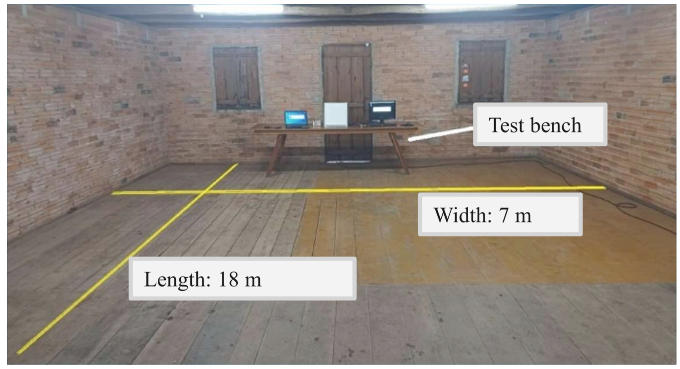

Fig. 3. Controlled bench test environment adapted in a laboratory room (18 m × 7 m) at Centro Universitário UniSATC. The Viaonda MID 12-iETH antenna was fixed to the test bench at the left end, and RFID-tagged sign replicas were approached frontally along the room length to characterize recognition distance and antenna beam coverage under repeatable conditions.

a 20 km/h MAXIMUM SPEED sign, located on the Centro Universitário UniSATC campus were selected. The RFID tags were attached to the supporting poles of the signs at an average height of 1.6 m, with a tolerance of approximately 20 cm, as shown in Fig. 4. For both environments, experimental protocols specified the number of repetitions, approach distances, vehicle speeds, and sign placement geometry. Each test condition was repeated multiple times to reduce random variability and to enable statistical analysis

Fig. 4. RFID tag installation on the supporting pole of a traffic sign on the UniSATC campus at a standardized mounting height of 1.6 m (±20 cm). Tags are encapsulated in ABS material with IP68 rating, designed for metallic surface installation compatible with standard sign poles. This mounting height was maintained consistently across all 12 field-test signs.

F. Vehicle Integration for Field Experiments

For field tests, the RFID antenna was mounted externally on a test vehicle using a custom support structure. The mounting position was selected to approximate a forward-facing perception configuration while maintaining mechanical stability and safety, as illustrated in Fig. 5. An onboard display and visual indicators were used solely to monitor system operation during experiments. These components did not influence the recognition process and were not involved in decision-making.

The experimental protocol is summarized as follows. A total of 24 passive UHF RFID tags were cataloged and mapped to three traffic sign categories: STOP, PEDESTRIAN CROSSING, and 20 km/h SPEED LIMIT. Bench experiments

Fig. 5. Integration of the RFID perception subsystem on the test vehicle for field experiments. The forward-facing Viaonda MID 12-iETH antenna is mounted on a custom external support structure on the vehicle roof. The Raspberry Pi processing unit, LED status indicators, and an onboard display monitor are installed inside the cabin solely for monitoring purposes; none of these components influenced the recognition results.

consisted of 120 controlled tag approaches, with each tag evaluated multiple times under frontal alignment and fixed orientation. Field experiments involved 12 tagged traffic signs distributed along a predefined university campus route, resulting in 60 measured approaches: each of the 12 signs was approached 5 times at an average speed of 10 km/h, yielding $n = 60$ total measurements. This design provides 5 replications per sign, which is considered acceptable given the observed variance (described in Section III-B). Additional dynamic runs were conducted qualitatively at 20 km/h and up to 40 km/h. The primary measured outputs were tag recognition occurrence and recognition distance, while lateral sign offset and roadway geometry were recorded as influencing factors.

III. Analysis and Results

This section presents the quantitative results obtained from bench and field experiments. The results are reported focusing on measured performance indicators such as recognition distance and detection consistency. Interpretation and implications are addressed in the Discussion section.

A. Bench Test Results

Bench tests were conducted to characterize system performance under controlled conditions. Each RFID tag was approached in a frontal configuration with consistent height and orientation. A total of n = 120 recognition distance measurements were collected. The system correctly presented the information associated with each tag on the graphical interface and in the activation of the digital outputs, as illustrated in Fig. 6.

Statistical analysis was performed assuming a normal distribution of recognition distances. The mean recognition distance obtained was 10.35 m, with a standard deviation of 0.97 m. The corresponding 95 % confidence interval was ±0.40 m. Confidence intervals were computed assuming normal distribution using the Student's t-distribution [15]. The statistical indicators obtained from the bench tests are presented in Table I.

Additional measurements evaluated recognition distance as a function of lateral offset. Recognition distance decreased

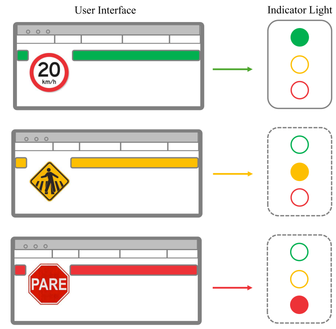

Fig. 6. System output during the bench test for three sign categories detected simultaneously. Left column shows the graphical interface panels for the 20 km/h speed limit sign, pedestrian crossing sign, and STOP sign (top to bottom). Right column shows the corresponding GPIO indicator lights activated on the Raspberry Pi for each detected sign, demonstrating correct multi-tag identification and priority-based output.

TABLE I

Statistical Characterization of RFID Recognition Distance under Controlled Bench Test Conditions (N = 120 Approaches, Frontal Tag Alignment, Fixed Orientation), including Standard Deviation, Mean, and 95% Confidence Interval Computed using the Student's T-Distribution

Standard Deviation (m)	0.971
Mean Distance (m)	10.353
Confidence Level (%)	95
Confidence Interval (m)	±0.396

progressively as lateral displacement increased, and no detections were observed beyond the antenna beamwidth limits. These distance measurements enabled the development of the antenna's effective reading coverage area and the identification of the regions with the highest efficiency, as illustrated in Fig. 7.

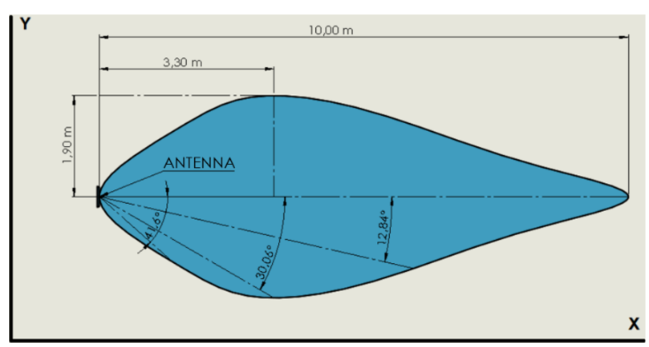

Fig. 7. Effective reading coverage area of the Viaonda MID 12-iETH antenna, derived from the bench test recognition distance measurements. The shaded region represents the operational detection envelope defined by the antenna's 42° beamwidth and a maximum detection range of approximately 10 m along the boresight axis. Lateral offset beyond 3.3 m at the antenna plane effectively reduces the detection zone, consistent with field test observations.

Simultaneous tag detection tests confirmed that multiple tags within the antenna field could be identified without misclassification. When tags associated with different sign categories were detected concurrently, a priority-based decision logic ensured consistent output behavior, as illustrated in Fig. 8.

Fig. 8. Simultaneous identification of multiple RFID tags representing different sign categories during bench tests. Each panel in the graphical interface corresponds to one detected tag, displayed in priority order (top to bottom: highest priority). The system correctly identifies all three signs without misclassification, demonstrating the reliability of the EPCglobal C1G2 Slotted ALOHA anti-collision protocol for multi-tag scenarios within the tested antenna envelope.

When three tags associated with different signs were approached, the system behaved similarly, presenting on the interface each sign corresponding to its respective tag. To prevent conflicts in sign identification and information processing, priority levels were implemented in the program so that the system recognizes the STOP SIGN as priority 1, the PEDESTRIAN CROSSING SIGN as priority 2, and the 20 km/h SPEED SIGN as priority 3, as shown in Fig. 9.

Fig. 9. Priority-based arbitration during concurrent detection of a STOP sign (priority 1) and a PEDESTRIAN CROSSING sign (priority 2). The interface highlights the highest-priority sign in the top row and lists remaining detected signs below, with their respective EPC codes, priority levels, and sign descriptions. This arbitration logic is extended in Section IV-C to support inter-sensor conflict resolution.

B. Field Test Results

Field tests were conducted along a predefined campus route containing multiple traffic signs equipped with RFID tags. Tags were applied to 5 STOP signs, 6 MAXIMUM SPEED 20 km/h signs, and 1 PEDESTRIAN CROSSING sign. These signs constitute the roadside signaling along the route defined by the red line. This information is correlated with the Google Maps image, as depicted in Fig. 10.

Dynamic tests were performed at vehicle speeds of up to 40 km/h. The initial quantitative test on the route was performed at an average speed of 10 km/h to facilitate the necessary measurements during sign identification; the vehicle stopped at each sign, and the recognition distance and the sign-to-road

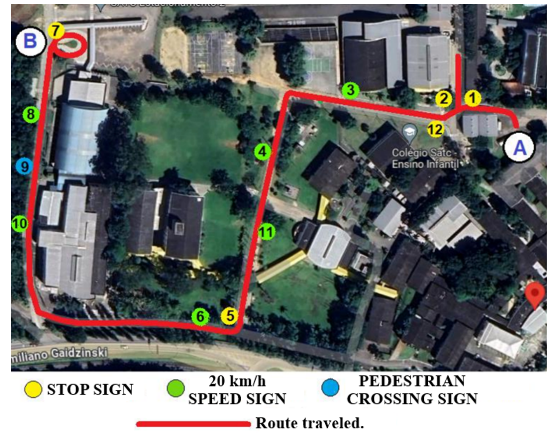

Fig. 10. Aerial view (Google Maps) of the predefined field test route on the Centro Universitário UniSATC campus (red line, approximately 800 m). Yellow markers indicate the 5 STOP signs, light-green markers the 6 maximum speed 20 km/h signs, and the highlighted marker the 1 PEDESTRIAN CROSSING sign. Sign numbers correspond to Table II. Letters A and B indicate the route start and end points.

lateral offset were measured, as presented in Table II. This procedure was executed five times per sign, resulting in a total of 60 approaches (12 signs × 5 repetitions).

TABLE II
PER-SIGN RECOGNITION DISTANCES AND LATERAL OFFSETS MEASURED DURING FIELD EXPERIMENTS AT 10 KM/H ON THE PREDEFINED UNISATC CAMPUS ROUTE. EACH OF THE 12 SIGNS WAS APPROACHED 5 TIMES, YIELDING N = 60 TOTAL MEASUREMENTS. SIGNS 6 AND 7 ARE LOCATED ON CURVED ROAD SEGMENTS, WHICH CONTRIBUTES TO THEIR REDUCED RECOGNITION DISTANCES

Sign No.	Recognition Distance (m)	Sign Lateral Offset (m)
1	12	1.0
2	10	1.5
3	9	2.0
4	4	3.5
5	10	1.5
6	3	1.5
7	5	1.5
8	10	1.5
9	10	1.5
10	10	1.5
11	5	3.0
12	10	1.5

*Recognition Distances in Curved Segments

Recognition distances ranged from 3 m to 12 m across all tested configurations. The mean recognition distance was 8.17 m, with a standard deviation of 2.906 m and a 95 % confidence interval of ±1.05 m, shown in Table III. A Shapiro-Wilk normality test applied to the 60-measurement dataset yielded a test statistic of $W = 0.94$ ($p = 0.07$), supporting the normality assumption at the 5 % significance level. This validates the use of parametric statistical methods, including confidence intervals and the probabilistic safety analysis presented in Section IV-B.

TABLE III
AGGREGATE STATISTICAL RESULTS FOR FIELD TEST RECOGNITION DISTANCES ($n = 60$), INCLUDING NORMALITY CONFIRMATION VIA SHAPIRO-WILK TEST ($W = 0.94$, $p = 0.07$) AND MINIMUM AND MAXIMUM OBSERVED VALUES WITH CORRESPONDING SIGN IDENTIFIERS

Standard Deviation (m)	2.906
Mean Distance (m)	8.167
Confidence Level (%)	95
Confidence Interval (m)	±1.053
Min. observed distance (m)	3.0 (sign 6, curved)
Max. observed distance (m)	12.0 (sign 1, offset 1.0 m)

Inspection of Table II reveals a clear dependence of recognition distance on lateral offset. Signs with lateral offsets of 1.0-1.5 m achieved recognition distances of 9-12 m, while signs at offsets of 3.0-3.5 m yielded distances of 4-5 m. A Pearson correlation analysis between recognition distance and lateral offset, computed from the 12 sign measurements in Table II, yields r = -0.87 ($p < 0.001$), confirming a strong negative linear relationship. This quantitative relationship is consistent with the directional characteristics of the antenna radiation pattern: the 42° beamwidth restricts effective coverage to signs within approximately 2.5 m lateral offset at typical roadside geometry.

All tagged traffic signs positioned within the antenna's effective coverage area along the vehicle trajectory were detected during the experiments. No detections were observed for signs positioned on the opposite side of the roadway. No false positive detections were recorded during the test sessions across all 60 approaches and all qualitative high-speed runs.

To complement the quantitative measurements at 10 km/h, additional dynamic runs were performed at 20 km/h and 40 km/h. Table IV presents the observed read rate, defined as the ratio of successful detection events to total passing events, across all three speed conditions.

TABLE IV
OBSERVED READ RATE (SUCCESSFUL DETECTIONS / TOTAL PASSING EVENTS) AT EACH TESTED VEHICLE SPEED. AT 20 KM/H AND 40 KM/H, TESTS WERE QUALITATIVE; RECOGNITION DISTANCE WAS NOT MEASURED. RESULTS APPLY TO SIGNS WITHIN THE ANTENNA'S GEOMETRIC ENVELOPE (LATERAL OFFSET 1.0–2.0 M, STRAIGHT SEGMENTS)

Speed (km/h)	Test type	Signs	Passes per sign	Total passes	Read rate
10	Quantitative	12	5	60	100%
20	Qualitative	12	3	36	100%*
40	Qualitative	12	3	36	100%*

*Read rate from qualitative passes; recognition distance not measured. Applies to signs within the antenna's geometric envelope (lateral offset 1.0–2.0 m on straight segments).

It is important to note that the present evaluation focuses on recognition occurrence and distance rather than end-to-end system latency. The adopted fixed reading interval of 500 ms was empirically selected to ensure stable operation and correct tag discrimination, introducing a trade-off between detection robustness and temporal resolution that is characterized analytically in Section IV.

IV. DISCUSSION

The experimental results confirm that RFID technology can reliably support traffic sign identification when employed as a redundant perception layer in autonomous mobility systems. Bench tests demonstrated recognition distances consistent with manufacturer specifications, while field experiments revealed reduced mean distances and increased variability. This discrepancy is primarily explained by non-ideal geometric alignment, vehicle motion, and dynamic antenna–tag orientation, which are intrinsic to real-world operation.

Recognition performance was shown to be strongly dependent on lateral sign offset, reflected in the Pearson correlation of $r = -0.87$ between recognition distance and lateral offset (Section III-B). These results indicate that system performance should be defined in terms of an effective operational envelope rather than maximum reading range. From an infrastructure perspective, modest adjustments in sign placement or antenna orientation can significantly improve reliability without requiring hardware modifications.

A. Protocol-Level Analysis: Dwell Time and Slotted ALOHA

The EPCglobal Class 1 Generation 2 (C1G2) protocol employed by the reading system uses a Slotted ALOHA anti-collision mechanism in which tags randomly select a response slot from a set of 2^Q slots per inventory round, where Q is the session parameter configured by the reader. For the Viaonda MID 12-iETH operating with $Q = 2$, each inventory cycle comprises 4 slots at approximately 3 ms per slot, yielding a cycle duration of $t_{cycle} \approx 12ms$.

The critical constraint for mobile readers is the dwell time, the duration during which a tag remains within the antenna's effective radiation pattern, which decreases with vehicle speed:

$$t_{dwell} = \frac{d_{recognition}}{v} \tag{1}$$

Table V presents the dwell time and the number of available ALOHA inventory cycles for the mean and minimum observed recognition distances at each tested speed. The compound detection probability, accounting for both ALOHA success within cycles and the probability that the 500 ms polling trigger fires within the dwell window, is:

$$P(detection) = \left[1 - \left(1 - \frac{1}{2^Q}\right)^{n_{cycles}}\right] \times min\left(\frac{t_{dwell}}{T_{poll}}, 1\right) \tag{2}$$

At 40 km/h and the minimum observed recognition distance of 3.0 m (sign 6, curved segment), the dwell time of 270 ms falls below the 500 ms polling interval, creating a deterministic vulnerability: the tag may traverse the entire detection zone between two consecutive polling triggers. This is distinct from ALOHA packet loss, it is a polling-layer miss that precedes the protocol layer entirely, and represents the primary protocol-level risk of the current implementation.

Within the ALOHA layer itself, for recognition distances that fall within the polling window, performance remains robust. At 40 km/h and 8.17 m recognition distance (61 available

TABLE V
DWELL TIME ANALYSIS AND EPCGLOBAL C1G2 SLOTTED ALOHA DETECTION PROBABILITY AT EACH TESTED SPEED, COMPUTED FOR THE MEAN FIELD RECOGNITION DISTANCE (8.17 M) AND THE MINIMUM OBSERVED DISTANCE (3.0 M). THE COMPOUND DETECTION PROBABILITY ACCOUNTS FOR BOTH ALOHA SUCCESS PROBABILITY WITHIN INVENTORY CYCLES AND THE RISK OF THE POLLING TRIGGER NOT FIRING WITHIN THE DWELL WINDOW

Speed	t_{dwell} (d=8.17 m)	t_{dwell} (d=3.0 m)	Dwell >500 ms?	Cycles (d=8 m)	Cycles (d=3 m)	P_{det} (d=8 m)	P_{det} (d=3 m)
10 km/h	2940 ms	1080 ms	Both	245	90	>99.9%	>99.9%
20 km/h	1470 ms	540 ms	Both	122	45	>99.9%	>99.9%
30 km/h	980 ms	360 ms	Both	81	30	>99.9%	>99.9%
40 km/h	735 ms	270 ms	d=8 m only	61	22	>99.9%	54–92%*
60 km/h	490 ms	180 ms	Neither	40	15	78–94%*	<30%*

*Includes polling window risk — depends on temporal alignment between polling trigger and dwell window.

cycles, per-cycle probability 25 %), the detection probability exceeds 99.9 %. The proposed mitigation, reducing the polling interval from 500 ms to 50–100 ms, requires no hardware modification and resolves the dwell-window vulnerability at all observed recognition distances for speeds up to 60 km/h. At 100 ms polling and 40 km/h, the worst-case sign (3.0 m, dwell = 270 ms) covers at least 2 polling opportunities, raising detection probability above 95 %.

B. Safety Margin Analysis and Worst-Case Bounds

For systems with safety-critical implications, mean performance characterization is insufficient; deterministic bounds and probabilistic guarantees over the recognition distance distribution are required. This section derives both from the experimental datasets.

At vehicle speed v, the total minimum distance required for a controlled stop after sign detection comprises two terms: the distance traveled during detection latency, and the kinematic braking distance:

$$d_{total} = d_{lat} + d_{brake} = v \times T_{poll} + \frac{v^2}{2a} \quad (3)$$

At 40 km/h (11.11 m/s) with $T_{poll} = 0.500s$ and $a = 6m/s$ (standard emergency deceleration): $d_{lat} = 5.56m$ and $d_{brake} = 10.3m$, yielding $d_{total} = 15.86m$. With ABS-assisted braking ($a = 8m/s^2$): $d_{brake} = 7.7m$ and $d_{total} = 13.26m$. Both values significantly exceed the mean field recognition distance of 8.17 m, confirming that the system cannot be used as a direct emergency braking trigger at 40 km/h. Table VI presents this analysis across the tested speed range.

The probabilistic safety guarantee - the probability that a given detection event provides sufficient distance for a safe stop - is derived from the normal distribution of field recognition distances ($\mu = 8.17m$, $\sigma = 2.906m$, normality confirmed by Shapiro-Wilk):

$$P(safe|v) = P(d_{rec} > d_{lat} + d_{brake}) = 1 - \Theta\left(\frac{(d_{total}(v) - \mu)}{\sigma}\right) \quad (4)$$

This yields: $P(safe|10km/h) = 98.3\%$, $P(safe|20km/h) = 92.7\%$, $P(safe|30km/h) = 27.1\%$, $P(safe|40km/h) < 2\%$. For worst-case recognition distances, the fifth percentile is $d_{rec}(P05) = \mu + \sigma\Theta^{-1}(0.05) = 3.39m$, consistent with the minimum observed value of 3.0 m. The first percentile yields $d_{rec}(P01) = 1.41m$.

These results lead to a fundamental design conclusion: the RFID subsystem as implemented is suitable as a direct braking-layer input only at speeds up to approximately 20 km/h. At higher speeds, the correct operational mode is anticipatory: the vehicle reduces speed when approaching known sign zones based on HD-map priors, with RFID confirmation arriving as corroborating evidence within the detection envelope. Under this model, the vehicle is already traveling at a reduced speed when RFID detection occurs, shifting the effective analysis to the 10–20 km/h rows of TableVI. This is entirely consistent with the system's proposed role as a redundant perception layer.

C. Bayesian Sensor Fusion Framework

Although implementation of a complete sensor fusion module is beyond the scope of this study, the theoretical contribution of the proposed architecture is strengthened by a formal characterization of how RFID outputs would be combined with vision-based detection within a Bayesian framework.

Let H denote the hypothesis that a traffic sign of type T is present at the vehicle's current location, with prior probability $P(H)$ derived from a geo-referenced HD map. Two independent binary observations are available: $R \in 0, 1$ (RFID detection) and $V \in 0, 1$ (vision detection). Under the conditional independence assumption - justified by the orthogonal failure modes of the two sensors - the posterior is:

$$P(H|R, V) = P(R|H)P(V|H)\frac{P(H)}{P(R, V)} \quad (5)$$

The field test dataset provides direct estimates for the RFID likelihood parameters. The detection probability $P(R = 1|H)$ is 1.0 for all signs within the antenna's geometric envelope, confirmed across all 60 field approaches. The false positive rate $P(R = 1|\neg H)$ was zero across all experimental sessions. This near-zero false positive rate is a structural property of the passive UHF RFID architecture: a tag can only be activated by a sufficiently strong RF field, and EPC codes are uniquely mapped to sign categories, precluding random triggering. Vision likelihood parameters $P(V = 1|H)$ and $P(V = 1|\neg H)$ are taken from published traffic sign recognition literature, with reported detection rates of 0.85–0.96 under favorable

TABLE VI
QUANTITATIVE SAFETY MARGIN ANALYSIS: TOTAL STOPPING DISTANCE REQUIRED AT EACH VEHICLE SPEED (LATENCY DISTANCE d_{lat} + BRAKING DISTANCE d_{brake}) COMPARED AGAINST THE MEAN FIELD RECOGNITION DISTANCE OF 8.17 M, FOR STANDARD DECELERATION ($a = 6m/s^2$) AND ABS-ASSISTED BRAKING ($a = 8m/s^2$). THE SYSTEM IS ADEQUATE FOR DIRECT BRAKING ACTUATION ONLY AT SPEEDS ≤ 20 KM/H

Speed(km/h)	d_{lat} 500ms (m)	d_{brake} a=6 (m)	d_{brake} a=8 (m)	d_{total} a=6 (m)	d_{total} a=8 (m)	$d_{recogmean}$ (m)	Adequate?
10	1.39	0.64	0.48	2.03	1.87	8.17	Yes
20	2.78	2.57	1.93	5.35	4.71	8.17	Yes
30	4.17	5.78	4.34	9.95	8.51	8.17	Marginal
40	5.56	10.30	7.70	15.86	13.26	8.17	No
60	8.33	23.15	17.36	31.48	25.69	8.17	No

conditions and false positive rates of 0.02–0.08 [1], [5], [6], [16].

TableVII presents the posterior $P(H|R,V)$ for each combination of sensor outputs, computed with representative parameter values $P(R = 1|H) = 1.0$, $P(R = 1|\neg H) = 0.0$, $P(V = 1|H) = 0.85$, $P(V = 1|\neg H) = 0.05$, prior P(H) = 0.70.

TABLE VII
BAYESIAN POSTERIOR PROBABILITY $P(H|R,V)$ FOR EACH COMBINATION OF RFID (R) AND VISION (V) SENSOR OUTPUTS, COMPUTED WITH EXPERIMENTALLY DERIVED PARAMETERS ($P(R = 1|H) = 1.0$, $P(R = 1|\neg H) = 0.0$, $P(V = 1|H) = 0.85$, $P(V = 1|\neg H) = 0.05$, $P(H) = 0.70$). THE TABLE SPECIFIES THE CORRESPONDING CONFIDENCE CLASSIFICATION AND RECOMMENDED VEHICLE ACTION FOR EACH SENSOR STATE

State	R	V	P(H—R,V)	Confidence	Vehicle Action
Full consensus	1	1	0.98	High	Proceed normally
RFID only	1	0	0.80	Medium-high	Comply + alert
Vision only	0	1	0.65	Medium	Reduce speed + alert
Neither detects	0	0	0.08	Low	Check map prior
Type conflict	A	B	—	Conflict	Most restrictive rule

The most consequential result is the asymmetry between single-sensor states. When RFID detects but vision fails ($R = 1, V = 0$), the scenario of a weathered or occluded sign undetected by the camera, the posterior reaches 0.80, providing sufficient confidence for sign compliance. This result follows directly from the experimentally verified zero false positive rate: RFID detections carry strong evidential weight even without vision confirmation. When vision detects but RFID misses ($R = 0, V = 1$), the posterior is lower (0.65) due to the nonzero false positive rate of vision classifiers. This asymmetry formally justifies treating RFID detections as higher-quality evidence than vision-only detections.

For type-conflict resolution, when both sensors detect but disagree on sign category, an explicit arbitration rule is specified: apply the most restrictive regulatory interpretation. The priority ordering already implemented (STOP > PEDESTRIAN CROSSING > SPEED LIMIT) extends naturally from multi-tag arbitration to inter-sensor conflict resolution, consistent with fail-safe design principles [17]. The three-state vehicle action mapping, normal operation ($P \geq 0.90$), precautionary speed reduction ($0.50 \leq P < 0.90$), and minimal-risk condition ($P < 0.50$ with nonzero map prior) - provides a concrete implementation framework for the arbitration logic.

D. Hazard Analysis (FMEA)

A simplified Failure Mode and Effects Analysis (FMEA) is presented in Table VIII to characterize the safety argument quantitatively. Severity (S), Occurrence (O), and Detectability (D) are scored on a 1–10 scale; $RiskPriorityNumber(RPN) = SOD$. Values are qualitative estimates based on experimental observations and domain knowledge. A conceptual arbitration framework for the proposed system is depicted in Fig. 11.

TABLE VIII
SIMPLIFIED FAILURE MODE AND EFFECTS ANALYSIS (FMEA) FOR THE RFID-BASED PERCEPTION LAYER. SIX FAILURE MODES ARE EVALUATED USING SEVERITY (S), OCCURRENCE (O), AND DETECTABILITY (D) SCORES ON A 1–10 SCALE, YIELDING THE RISK PRIORITY NUMBER ($RPN = SOD$). LATENCY EXCEEDING THE SAFETY THRESHOLD ($RPN = 144$) IS THE SOLE CRITICAL RISK AND IS MITIGATED BY THE ANTICIPATORY OPERATIONAL DESIGN

Failure Mode	Effect	S	O	D	RPN
RFID missed detection	Vision-only fallback	4	3	2	24
RFID false positive	Incorrect sign output	7	1	3	21
Vision failure	RFID as primary	4	4	2	32
RFID–Vision conflict	Ambiguous sign identity	8	1	2	16
Latency exceeds safety threshold	Insufficient stopping distance >20 km/h	9	4	4	144
Dual-source failure	Complete loss of sign perception	9	1	2	18

The FMEA results confirm that latency exceeding the safety threshold (RPN = 144) is the only critical risk, as it directly impacts stopping distance at higher vehicle speeds, and is therefore mitigated through system-level design choices, including redefining RFID as an anticipatory perception layer, reducing the polling interval, and incorporating map-based

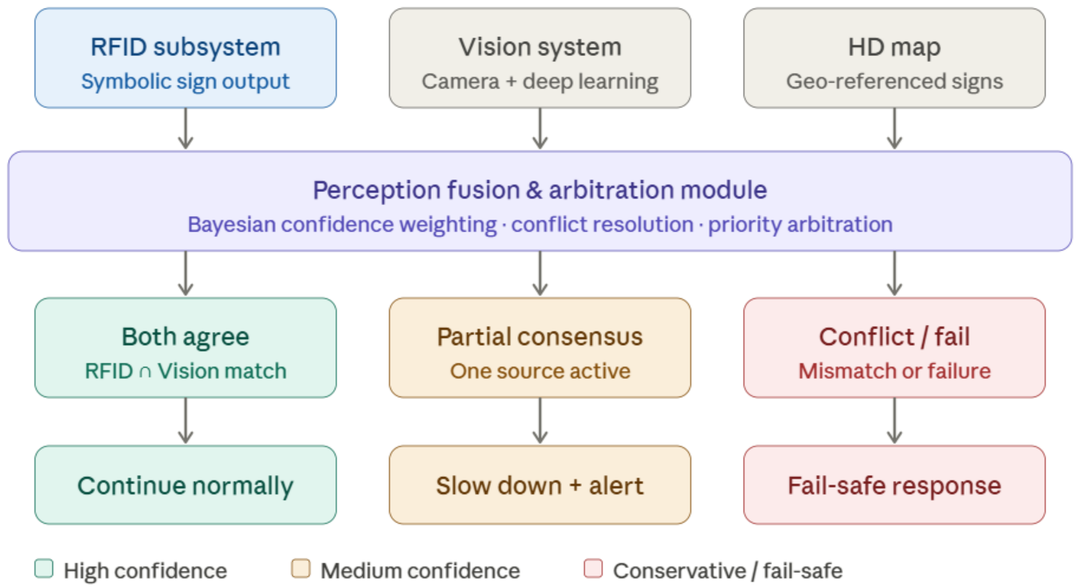

Fig. 11. Conceptual perception fusion and arbitration architecture proposed for integration of the RFID subsystem with vision-based and map-based perception modules. Three input sources (RFID subsystem, vision system, HD map) feed into a Bayesian confidence weighting and conflict resolution module. The three resulting confidence states, full consensus (RFID $\bigcap$ Vision match), partial consensus (one source active), and conflict/fail (mismatch or dual failure), map to corresponding vehicle responses: continue normally, slow down and alert, or activate fail-safe behavior. See Section IV-C and Table VII for the quantitative Bayesian formulation.

pre-alerting, as discussed in Section IV-B. All other failure modes present RPN values below 40 and are effectively mitigated at the perception and arbitration layers through redundancy mechanisms such as fallback to vision, cross-validation with map data, and fail-safe strategies based on the most restrictive rule. Moderate-risk conditions, such as vision system failure (RPN = 32), are inherently addressed by the proposed architecture, where RFID provides an independent perception channel, while low-risk events—including RFID missed detection (RPN = 24), false positives (RPN = 21), RFID–vision conflict (RPN = 16), and dual-source failure (RPN = 18)—are controlled through established redundancy and arbitration logic. Notably, the false positive scenario is further supported by experimental evidence, as no false detections were observed in field tests, reinforcing the robustness of the proposed approach.

E. Environmental Robustness and Multipath Considerations

The proposed RFID-based approach exhibits structural independence from optical conditions that distinguishes it from vision-based systems. UHF radio frequency signals in the 902–928 MHz band are not affected by ambient lighting, fog, or occlusion. Precipitation introduces a small additional path loss, typically in the range of 0.01 dB/km per mm/h of rainfall, which is negligible at the detection distances reported in this study (3-12 m). Temperature effects are bounded by the tag specification (-30 °C to 80 °C), covering the operational range of Brazilian outdoor environments.

In real-world environments, however, UHF signals in the 900 MHz band are susceptible to multipath fading caused by reflections from metallic surfaces such as parked vehicles, guard rails, and fences. Destructive interference between reflected and direct-path signals can produce null zones within the nominal detection envelope, potentially explaining the reduced recognition distances observed at signs 6 and 7 (curved segments, 3 m and 5 m respectively). The present study did not implement RSSI-based filtering or multipath mitigation. Whether the low recognition distances at these signs result from geometric curvature, multipath effects, or their combination cannot be determined from the available data. Future work should include RSSI logging, available via the TCP/IP interface of the Viaonda reader, to characterize and mitigate multipath effects, ensuring that the reported mean detection distance remains consistent across diverse infrastructure layouts.

F. System Integration and Deployment Constraints

RFID-based traffic sign identification should be regarded as complementary to vision-based perception rather than a replacement. The dominant limitations of the proposed approach are geometric and infrastructural rather than environmental: recognition performance is mainly affected by antenna orientation, lateral displacement, and roadway curvature. Consequently, RFID-assisted perception is best suited for controlled or semi-controlled environments, campuses, industrial zones, and smart city corridors, where infrastructure placement can be managed [18].

The modular architecture of the RFID subsystem facilitates integration with existing autonomous platforms by providing symbolic outputs compatible with sensor fusion frameworks [19]. Despite its feasibility, the approach requires infrastructure modification and raises security considerations, such as unauthorized tag reading and signal interference [20], which were beyond the scope of this study.

V. Conclusion

This paper presented the design, experimental evaluation, and formal safety analysis of an RFID-based traffic sign identification system intended to function as a redundant perception layer for autonomous mobility applications. Passive UHF RFID tags were integrated into traffic signs, and a vehicle-mounted reader system was evaluated under controlled laboratory conditions and semi-controlled real-world environments.

Experimental results demonstrated reliable traffic sign identification within a defined operational envelope, with recognition distances strongly influenced by lateral offset ($r = -0.87$) and road geometry. Bench tests yielded a mean recognition distance of 10.35 m; field tests confirmed reliable detection at up to 40 km/h with a mean distance of 8.17 m and zero false positive detections across all sessions.

A quantitative safety margin analysis establishes that the system provides probabilistic safety guarantees for emergency braking at speeds up to 20 km/h ($P = 92.7\%$), and should be operated as an anticipatory redundant layer at higher speeds, consistent with the system's proposed role throughout this work. A dwell time analysis characterizes the Slotted ALOHA protocol performance across the tested speed range, identifying the 500 ms polling interval as the primary vulnerability for signs with short recognition distances at speeds above 30 km/h, and proposing polling interval reduction as a software-level mitigation. A Bayesian sensor fusion framework, parametrized from the experimental false positive rate of zero, formalizes the complementary roles of RFID and vision sensors and specifies conflict resolution rules for each possible sensor state combination. A simplified FMEA identifies latency as the critical risk ($RPN = 144$) and confirms that all other failure modes are mitigable at the arbitration layer.

Future work will address: (i) quantitative latency measurement from tag read to GPIO activation under static and dynamic conditions; (ii) controlled braking trials combining instrumented vehicle deceleration data with RFID detection events at 20, 40, and 60 km/h; (iii) RSSI-based multipath characterization and filtering; (iv) reduction of the polling interval to 50–100 ms to resolve the dwell-window vulnerability at higher speeds; (v) dense infrastructure experiments evaluating read rate and arbitration latency with sign spacing below 10 m; and (vi) empirical validation of the Bayesian fusion framework through co-deployment of the RFID subsystem with a vision-based classifier.

Acknowledgments

This study was financed in part by the Fundação de Amparo à Pesquisa e Inovação do Estado de Santa Catarina (FAPESC) – FAPESC 21/2024.

References

[1] S. Sivaraman and M. M. Trivedi, "Looking at vehicles on the road a survey of vision-based vehicle detection, tracking, and behavior analysis," *IEEE Transactions on Intelligent Transportation Systems*, vol. 14, no. 4, pp. 1773–1795, Dec. 2013, doi: 10.1109/TITS.2013.2266661.

[2] C. Olaverri-Monreal and T. Jizba, "Autonomous vehicles and smart mobility-related technologies," *Journal of Advanced Transportation*, vol. 2021, p. 9111820, 2021, doi: 10.1155/2021/9111820.

[3] SAE International, *Taxonomy and Definitions for Terms Related to Driving Automation Systems for On-Road Motor Vehicles (J3016)*, Std., 2021, doi: 10.4271/J3016_202104.

[4] M. Buehler, K. Iagnemma, and S. Singh, *The DARPA Urban Challenge: Autonomous Vehicles in City Traffic*. Berlin, Germany: Springer, 2009, doi: 10.1007/978-3-642-03991-1.

[5] J. e. a. Su, "Traffic sign recognition using vision-radar sensor fusion for autonomous vehicles," *IEEE Transactions on Intelligent Transportation Systems*, vol. 25, no. 3, pp. 2116–2129, 2024, doi: 10.1109/TITS.2023.3317242.

[6] K. e. a. Eykholt, "Robust physical-world attacks on deep learning visual classification," in *Proceedings of the IEEE/CVF Conference on Computer Vision and Pattern Recognition (CVPR)*, 2018, doi: 10.1109/CVPR.2018.00175, pp. 1625–1634.

[7] Confederação Nacional do Transporte, "59,2% das rodovias brasileiras apresentam problemas de sinalização," Feb. 2018, accessed on Apr. 10, 2026. [Online]. Available: https://www.cnt.org.br/agencia-cnt/sem-saber-o-que-vem-pela-frente

[8] B. Pawłowicz, M. Salach, and P. Jankowski-Mihułowicz, "Dynamic rfid identification in urban traffic management systems," *Sensors*, vol. 20, no. 15, p. 4225, 2020, doi: 10.3390/s20154225.

[9] S. C. M. de Alencar, K. H. D. de Lima, I. R. de S. Meireles, and Y. P. de Assis, "Estudo da influência da orientação espacial na potência do sinal rf irradiado por tags rfid uhf passivas," *Igapó*, vol. 19, no. 1, p. 700, 2025, doi: 10.31417/irecitecifam.v19.700.

[10] E. Uhlemann, "Introducing connected vehicles," *IEEE Vehicular Technology Magazine*, vol. 10, no. 1, pp. 23–31, 2015, doi: 10.1109/MVT.2015.2390920.

[11] J. Contreras-Castillo, S. Zeadally, and J. A. Guerrero-Ibanez, "Internet of vehicles: Architecture, protocols, and security," *IEEE Internet of Things Journal*, vol. 5, no. 5, pp. 3701–3709, 2018, doi: 10.1109/JIOT.2017.2690902.

[12] L. e. a. Bariah, "A prospective look: Key enabling technologies, applications and open research topics in 6g networks," *IEEE Access*, vol. 8, pp. 174 792–174 820, 2020, doi: 10.1109/ACCESS.2020.3019590.

[13] R. Molina-Masegosa and J. Gozalvez, "Lte-v for sidelink 5g v2x vehicular communications," *IEEE Vehicular Technology Magazine*, vol. 12, no. 4, pp. 30–39, 2017, doi: 10.1109/MVT.2017.2752798.

[14] R. Rajamani, *Vehicle Dynamics and Control*, 2nd ed. New York, NY, USA: Springer, 2012, doi: 10.1007/978-1-4614-1433-9.

[15] C. M. Patino and P. Onarden, "Intervalos de confiança: uma ferramenta útil para estimar o verdadeiro tamanho de efeito," *Jornal Brasileiro de Pneumologia*, vol. 41, no. 5, pp. 485–485, 2015, doi: 10.1590/S1806-37562015000000314.

[16] H. Durrant-Whyte and T. Bailey, "Simultaneous localization and mapping: Part i," *IEEE Robotics & Automation Magazine*, vol. 13, no. 2, pp. 99–110, 2006, doi: 10.1109/MRA.2006.1638022.

[17] H. Kopetz, *Real-Time Systems: Design Principles for Distributed Embedded Applications*, 2nd ed. New York, NY, USA: Springer, 2011, doi: 10.1007/978-1-4419-8237-7.

[18] A. Zanella, N. Bui, A. Castellani, L. Vangelista, and M. Zorzi, "Internet of things for smart cities," *IEEE Internet of Things Journal*, vol. 1, no. 1, pp. 22–32, 2014, doi: 10.1109/JIOT.2014.2306328.

[19] S. Thrun, W. Burgard, and D. Fox, *Probabilistic Robotics*. Cambridge, MA, USA: MIT Press, 2005, doi: 10.1007/978-3-031-11992-7.

[20] M. Agrawal and D. Bhurke, "Security threats in rfid-based systems: A comprehensive review," *Journal of Network and Computer Applications*, vol. 188, p. 103560, 2021, doi: 10.1016/j.jnca.2021.103560.

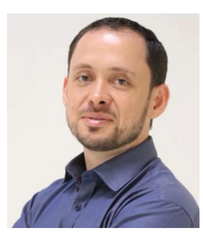

João Mota Neto Ph.D. degree in Mining, Metallurgy and Materials Engineering from the Federal University of Rio Grande do Sul (UFRGS) in 2017, M.S. degree in Mechanical Engineering from the Federal University of Rio Grande do Sul (UFRGS) in 2013 and Technologist in Industrial Automation from Faculdade SATC (FASATC) in 2011. Currently Undergraduate Course Coordinator for Mechatronics Engineering at UniSATC. His current and previous research interests include electro-electronic instrumentation, power generation from piezoelectric micro-energy sources, autonomous mobility, alternative energy sources, electrical circuits, and production engineering

Marcos Antônio Jeremias Coelho M.S. degree in Electrical Engineering from the Federal University of Rio Grande do Sul (UFRGS), Brazil, in 2015 and B.S. degree in Electrical Engineering from Faculdade SATC, Brazil, in 2013. Currently a Professor and Researcher in the Mechatronics Engineering program at University Center UniSATC, Criciúma, SC, Brazil. Has experience in Electrical Engineering, with an emphasis on Industrial Electronics and Electronic Systems and Controls. His current and previous research interests include electro-electronic instrumentation, power generation from piezoelectric micro-energy sources, autonomous mobility, alternative energy sources, and electrical circuits.

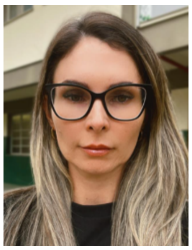

Gabriela Rocha Roque M.S. degree in information and communication technologies from the Federal University of Santa Catarina (UFSC), specialization in production engineering from the State University of Santa Catarina (UDESC), in 2010, and in psychopedagogy from Fundação Universidade Regional de Blumenau (FURB) and Technologist in Industrial Automation from Faculdade SATC (FASATC) in 2007. Currently a Professor and Researcher in the Mechatronics Engineering program at UniSATC, Criciúma, SC, Brazil. Areas of expertise and research interests include Robotics, Mechatronics, and Automation, Mechanical Engineering, Production Engineering, and Education, with a focus on Educational Technology.

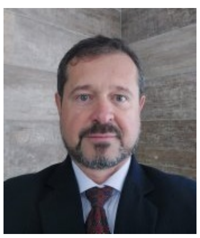

Roderval Marcelino M.S. degree and the Ph.D. degree in engineering from the Federal University of Rio Grande do Sul (UFRGS), Brazil and B.S. degree in computer science from the University of Southern Santa Catarina (UNISUL), Brazil, in 1998. Postdoctoral fellowship at ULSTER University in Northern Ireland. Currently at Professor with exclusive dedication at the Federal University of Santa Catarina (UFSC). He has experience in Computer Science, with an emphasis on Embedded Systems. He is the leader of the CNPQ research group CPS Lab (Cyber-Physical Systems Laboratory) and a member of the Brazilian Center for Mechanical/Metal Forming (UFRGS). His current and previous research interests include cyber-physical systems, AI at the edge, automation, renewable energy, and computational systems.